Chinese Chemical Letters 35 (2024) 108469

Contents lists available at ScienceDirect

Chinese Chemical Letters

journal homepage: www.elsevier.com/locate/cclet

Enhanced cycle stability of aprotic Li-O_2 batteries based on a self-defensed redox mediator

Guiru Sun[a,1], Yan Wang[a,1], Daming Yang[a], Zexu Zhang[a], Wei Lu[a,b], Ming Feng[a,*]

[a] Key Laboratory of Functional Materials Physics and Chemistry of the Ministry of Education, Jilin Normal University, Changchun 130103, China
[b] College of Information Technology, Jilin Engineering Research Center of Optoelectronic Materials and Devices, Jilin Normal University, Siping 136000, China

ARTICLE INFO

Article history:
Received 6 March 2023
Revised 23 March 2023
Accepted 18 April 2023
Available online 19 April 2023

Keywords:
$MgBr_2$
Redox mediator
Redox shuttle
Li anode
SEI film

ABSTRACT

LiBr as a promising redox mediator (RM) has been applied in Li-O_2 batteries to improve oxygen evolution reaction kinetics and reduce overpotentials. However, the redox shuttle of Br_3^- can induce the unexpected reactions and thus cause the degradation of LiBr and the corrosion of Li anode, resulting in the poor cyclability and the low round-trip efficiency. Herein, $MgBr_2$ is firstly employed with dual functions for Li-O_2 batteries, which can serve as a RM and a SEI film-forming agent. The Br^- is beneficial to facilitating the decomposition of Li_2O_2 and thus decreasing the overpotential. Additionally, a uniform SEI film containing Mg and MgO generates on Li anode surface by the *in-situ* spontaneous reactions of Mg^{2+} and Li anode in an O_2 environment, which can suppress the redox shuttle of Br_3^- and improve the interface stability of Li anode and electrolyte. Benefiting from these advantages, the cycle life of Li-O_2 battery with $MgBr_2$ electrolyte is significantly extended.

The rapid development of intelligent electronic equipment has aroused great research interest in the demand for high energy density secondary batteries [1–3]. Among the secondary batteries, lithium-oxygen (Li-O_2) battery with highest theoretical energy density (3500 Wh/kg) is regarded as a promising candidate [4]. The high theoretical energy density of Li-O_2 battery is related to the inherent electrochemical reactions [5]. During discharge, the O_2 undergoes an oxygen reduction reaction (ORR) to form a solid discharge product (Li_2O_2) [6]. During recharge, Li_2O_2 decomposes into O_2 and Li^+ by oxygen evolution reaction (OER) [7,8]. The generated Li_2O_2 can inevitably deposit on cathode and block the porous channel owing to its insulating and insoluble nature, which will lead to the high overpotential, giving rise to the low round-trip efficiency and short cycle life of Li-O_2 batteries [9–11].

To alleviate the high overpotential, some solid catalysts and redox mediators (RMs) were reported, which can improve the battery performance by promoting ORR and OER processes [12–14]. However, the limited connection interface of solid catalysts and Li_2O_2 leads to the incomplete decomposition of Li_2O_2, which hinders its practical application [15,16]. In contrast, RMs as charge carrier facilitate the Li_2O_2 decomposition by two-step reactions (RM $\leftrightarrow$ $RM^{ox} + e^-$ and $Li_2O_2 + RM^{ox} \rightarrow O_2 + RM + Li^+$) [17,18], which contributes to obtaining a reduced overpotential. To date, several types of RMs have reported, such as organic RMs [19,20], organometallic RMs [21], and halide RMs [22]. Among the RMs, halide RMs have attracted considerable attentions due to their merits, including simple synthesis, easy availability, and low cost, which mainly contains LiI and LiBr [23,24]. It has been reported that I^- suffers from a proton-consuming reaction in both protic and aprotic electrolytes, boosting the generation of the irreversible discharge products of LiOH and LiOOH [25]. In contrast, LiBr as a RM will not undergo a solvent deprotonation, leading to the formation of desirable discharge product of Li_2O_2 [26].

Previously, in a LiBr-containing Li-O_2 system, a bottleneck question is that the diffusible Br_3^- reacts with Li anode, which is named redox shuttle. The redox shuttle results in the degradation of LiBr and the corrosion of Li anode, leading to a poor cycle stability [27]. Recently, several self-defensed RMs have been reported to inhibit the redox shuttle of Br_3^-, such as *N*-methyl-*N*-propyl pyrrolidine bromide (MPPBr) [28], $InBr_3$ [29], and bromonitromethane ($BrCH_2NO_2$) [30], which not only can lower the overpotential by the redox couple of Br_3^-/Br^- but also can *in-situ* form a SEI film to protect Li anode against deterioration by Br_3^-. These formed SEI films are mainly by the *in-situ* spontaneous reactions between introduced RM and Li anode. Earlier studies have proposed that gas environments are keys to the formation of SEI film, especially in Li-O_2 batteries [31]. The obtained SEI film shows good stability based on the O_2-involved reaction in Li-O_2 batteries [32]. Therefore, it is

* Corresponding author.
E-mail address: mingfeng@jlnu.edu.cn (M. Feng).
[1] These authors contributed equally to this work.

https://doi.org/10.1016/j.cclet.2023.108469
1001-8417/

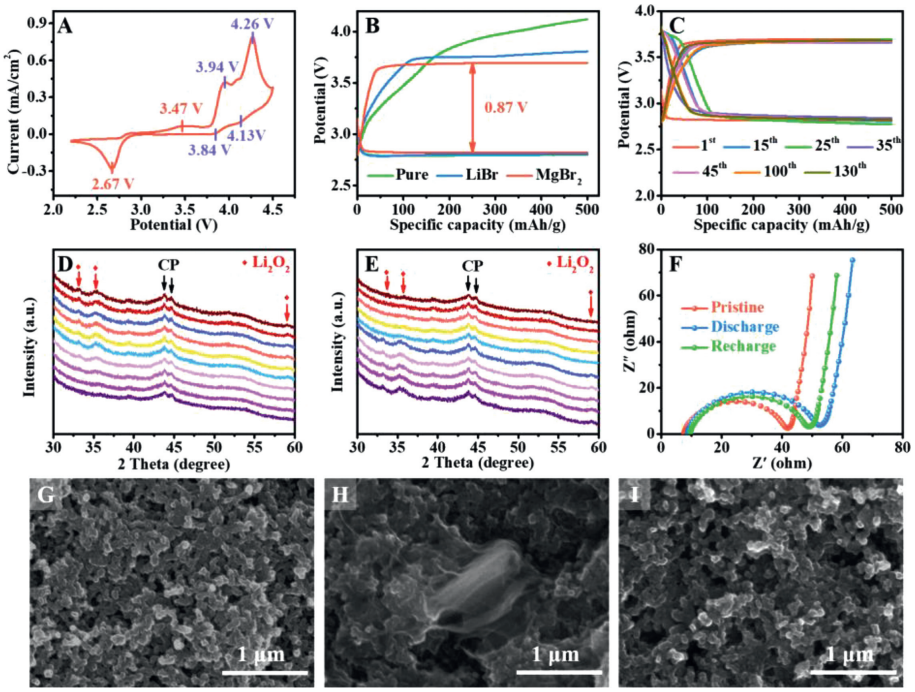

Fig 1. (A) CV profile of Li-O_2 battery with $MgBr_2$ electrolyte. (B) The first discharge/charge curves of Li-O_2 batteries with different electrolytes. (C) The cycling curves of battery with $MgBr_2$ electrolyte. *In-situ* XRD patterns of cathode in a Li-O_2 battery with $MgBr_2$ electrolyte during (D) discharge and (E) recharge. (F) Nyquist plots and (G-I) SEM images of cathodes at different electrochemical states for the Li-O_2 battery with $MgBr_2$ electrolyte.

significant to *in-situ* construct a table SEI film by O_2-involved reaction in a self-defensed RM-based Li-O_2 battery.

Herein, we firstly used $MgBr_2$ as a self-defensed RM for Li-O_2 batteries. The formed Br_3^- can boost the oxidization of Li_2O_2 and thus lower the overpotential. Equally, a uniform SEI film containing Mg and MgO forms on Li anode surface owing to the *in-situ* spontaneous reactions of Mg^{2+} and Li anode in an O_2 environment. The formed SEI film not only can inhibit the redox shuttle of Br_3^- but also can enhance the interface stability between Li anode and electrolyte. As expected, the cell with $MgBr_2$ electrolyte shows a long cycle life of 130 cycles.

Fig. 1A displays a cyclic voltammogram (CV) profile of Li-O_2 battery with $MgBr_2$ electrolyte. These are three pairs of redox peaks. One pairs of peaks at 2.67 and 3.47 V correspond to the Li_2O_2 formation and decomposition [33]. The other two pairs of peaks result from the reversible reaction of $Br^- \leftrightarrow Br_3^-$ (3.84 and 3.94 V) and $Br_3^- \leftrightarrow Br_2$ (4.13 and 4.26 V), respectively, which is similar to that of the battery with LiBr (Fig. S1 in Supporting information), indicating that the $MgBr_2$ can act as a RM to boost Li_2O_2 decomposition. The electrochemical performance of Li-O_2 battery with pure, LiBr, and $MgBr_2$ electrolytes is evaluated at a current density of 100 mA/g and a capacity limit of 500 mAh/g. The first discharge-charge curves of the Li-O_2 battery with different electrolytes are shown in Fig. 1B, which exhibits the similar discharge potential plateaus of ~2.80 V. The charge potential plateau of battery with pure, LiBr and $MgBr_2$ electrolyte is 3.75, 3.69 and 3.92 V, respectively. A low overpotential for the battery with $MgBr_2$ electrolyte is thus obtained, which is 0.87 V. Equally, the cycle life of the battery with $MgBr_2$ electrolyte reaches 130 cycles (Fig. 1C), which much higher than that of 80 cycles for the battery with LiBr electrolyte (Fig. S2 in Supporting information).

In order to assess the reversibility of battery with $MgBr_2$ electrolyte, the cathodes at different electrochemical states were characterized by *in-situ* X-ray diffraction (XRD), electrochemical impedance spectroscopy (EIS), and scanning electron microscopy (SEM). The *in-situ* XRD patterns of the discharged and recharged cathode are displayed in Figs. 1D and E. The new diffraction peaks at 32.7°, 34.9° and 58.5° appear and become stronger during discharge process, corresponding to the (201), (200) and (220) plane of Li_2O_2 (JCPDS No. 73–1640), respectively (Fig. 1D), proving that the discharge product is Li_2O_2 [34]. The intensity of these diffraction peaks gradually weakens until disappear during recharge process (Fig. 1E), demonstrating that the formed Li_2O_2 is completely decomposed. In Fig. 1F, the impedances of battery with $MgBr_2$ electrolyte are investigated at different electrochemical states using EIS. The corresponding resistances are 34.20, 44.15 and 39.60 Ω for a battery at pristine, discharge, and recharge, respectively. The increased resistance after discharge and the reduced resistance after recharge are attributed to the generation and oxidation of Li_2O_2, confirming the battery with $MgBr_2$ electrolyte exhibits good reversibility. The SEM image of the pristine cathode shows that the super P particles uniformly distribute on cathode surface (Fig. 1G). After discharge, the film-like discharge product is observed in Fig. 1H, suggesting that the generated Li_2O_2 is film-like. In Fig. 1I, the film-like Li_2O_2 is completely removed after recharge, further indicating that a Li-O_2 battery with superior reversibility is obtained by using $MgBr_2$ electrolyte.

The SEM images of cycled Li anode in Li-O_2 batteries with different electrolytes were gathered to insight into the effect of $MgBr_2$ on the Li anode, as shown in Fig. 2 and Fig. S3 (Supporting information). In Fig. S3, the pristine Li anode surface is flat and smooth. After first cycle, the cycled Li anode suffers from severer corrosion and its surface is rough for the battery with LiBr electrolyte (Fig. 2A), which could be caused by the redox shuttle of Br_3^- [35]. Note that the Li anode surface is coated with the SEI film comprised of the dense and uniform particles (Fig. 2B). The corresponding EDS element mapping images of the cycled Li anode in the battery with $MgBr_2$ electrolyte are shown in Fig. S4 (Supporting information). The elements of Mg, Br, O and C are uniformly distributed on the Li anode surface, proving that the formed SEI film consists of Mg, Br, O and C, which should mainly come from the $MgBr_2$-induced reaction. Additionally, the corrosion of Li anode becomes serious after 20th cycle for the battery with LiBr electrolyte (Fig. 2C). In contrast, there is no obvious corrosion for

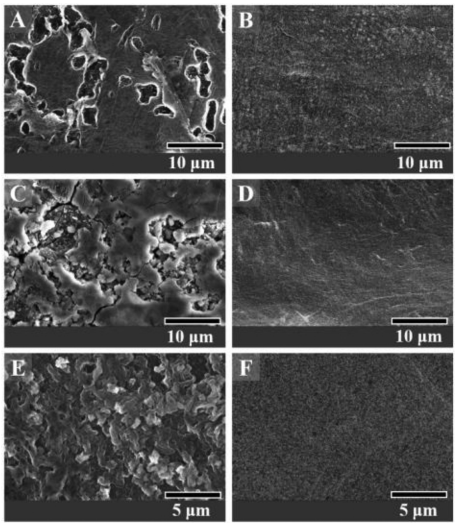

Fig. 2. SEM images of Li anodes in a Li-O_2 battery with (A, C, E) LiBr and (B, D, F) $MgBr_2$ electrolytes after different cycles.

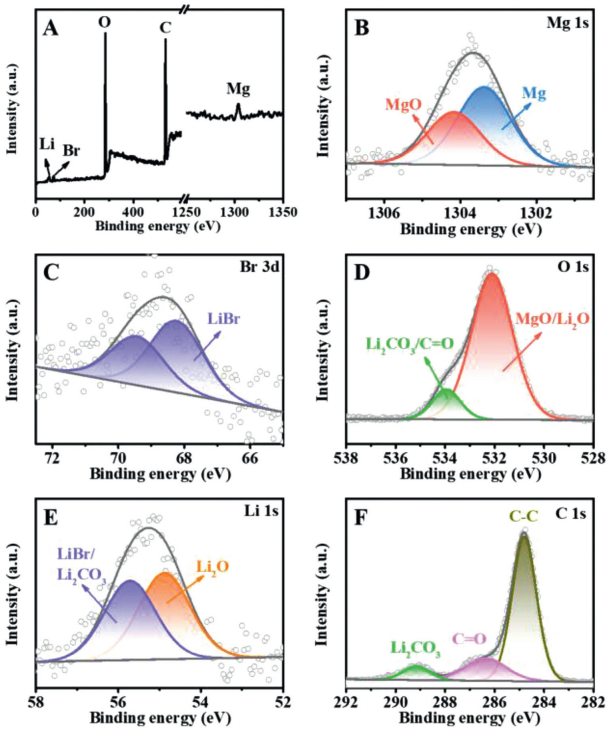

Fig. 3. (A) XPS survey spectrum and core-level spectra of (B) Mg 1s, (C) Br 3d, (D) O 1s, (E) Li 1s, and (F) C 1s for cycled Li anode in a Li-O_2 battery with $MgBr_2$ electrolyte after first cycle.

the Li anode cycled in the battery with $MgBr_2$ electrolyte after 20th cycle (Fig. 2D). After 50th cycle, the surface of Li anode is loosely packed (Fig. 2E), which is caused by the dead Li and corrosion reaction [36]. In Fig. 2F, the surface of cycled Li anode is smooth and dense after 50th cycle in the battery with $MgBr_2$ electrolyte. These results indicate that the SEI film resulted from $MgBr_2$-induced reaction can inhibit the redox shuttle of Br_3^-.

To identify the element compositions of formed SEI film, the cycled Li anode in the Li-O_2 battery with $MgBr_2$ electrolyte after first cycle was characterized by XPS (Fig. 3). The survey spectrum shows that the SEI film consists of C, O, Li, Br and Mg (Fig. 3A). In Fig. 3B, the Mg 1s spectrum exhibits two magnesium contributions, which represents the Mg metal (1303.4 eV) and MgO (1304.2 eV) [37], respectively. The Mg metal comes from the reduction of Mg^{2+} due to the Mg^{2+}/Mg with high standard reduction potential (0.67 V) than that of Li^+/Li [38]. The MgO is caused by the oxidation of Mg metal in O_2 environment [39]. As comparison, the Mg 1s spectrum of cycled Li anode in the Li|Li symmetric battery with $MgBr_2$ electrolyte under Ar atmosphere is gathered (Fig. S5 in Supporting information). The spectrum of cycled Li anode only shows one Mg metal peak at 1303.4 eV, which provides the solid evidence that the O_2 environment is a key to the formation of MgO. Fig. 3C displays the binding energies of Br $3d_{3/2}$ and Br $3d_{5/2}$ at 68.4 and 69.4 eV, corresponding to the Br^- [40], which results from the residual LiBr. In Fig. 3D, the O 1s spectrum is fitted with two peaks, which are the characteristic of MgO/Li_2O (532.1 eV) and Li_2CO_3/C=O (533.9 eV), respectively [41,42]. The Li 1s spectrum contains two peaks, which are attributed to Li_2O (54.9 eV) and LiBr/Li_2CO_3 (55.7 eV), respectively [29]. The C 1s spectrum is divided into three different peaks at 284.8, 286.4 and 289.2 eV, ascribing to the C–C, C=O and Li_2CO_3, respectively [32]. Compared with the XPS results of pristine Li anode (Fig. S6 in Supporting information), the formed SEI film is mainly composed of Mg and MgO, which is beneficial to inducing the homogeneous deposition of Li [43]. Equally, the XPS spectra of cycled Li anode in the Li-O_2 battery with $MgBr_2$ electrolyte after 20th were obtained. There is a little change for the composition of SEI film after 20th cycle (Fig. S7 in Supporting information), which suggests that the formed SEI film shows good stability.

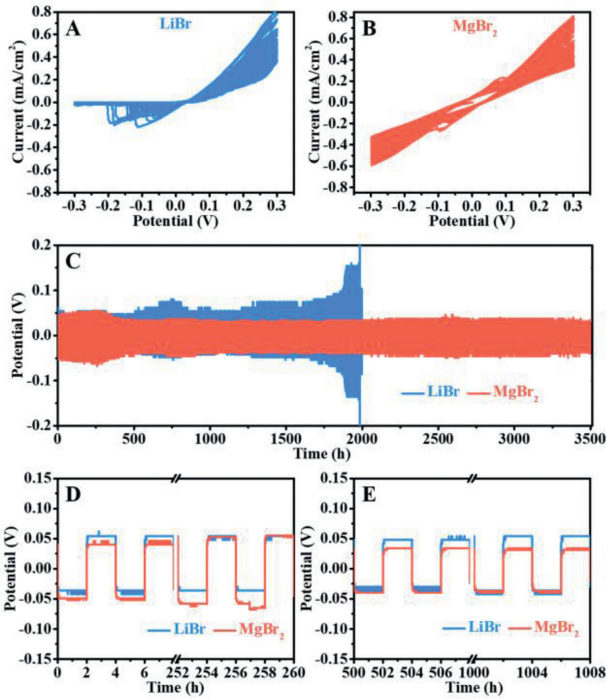

Fig. 4. (A, B) CV curves and (C-E) potential profiles of the Li|Li symmetric batteries with LiBr and $MgBr_2$ electrolyte.

In Fig. 4, the plating/stripping processes of Li|Li symmetric battery with LiBr and $MgBr_2$ electrolyte are studied in an O_2 atmosphere by CV and galvanostatic tests to insight into the influence of generated SEI film on the interface stability between Li anode and electrolyte. Figs. 4A and B present the CV curves of Li|Li symmetric battery with LiBr and $MgBr_2$ electrolytes, respectively. It can be seen that the battery with LiBr electrolyte shows a lower initial current density than that of the battery with $MgBr_2$ electrolyte. In addition, the current densities of the battery with LiBr electrolyte continuously reduce during 50 cycles, whereas only a little change of current density is found for the battery with $MgBr_2$ electrolyte, suggesting that the formed SEI film contributes to improving the

interface stability between the Li anode and electrolyte. The cycling performance of Li|Li symmetric batteries with LiBr and $MgBr_2$ electrolytes was tested at a current density of 0.05 mA/cm^2 and a limited capacity of 0.1 mAh/cm^2. In Fig. 4C, the Li|Li symmetric battery with LiBr electrolyte only cycles for 1980 h, while a longer cycle life of 3510 h is obtained for the battery with $MgBr_2$ electrolyte. The enlarged view of detailed potential profiles of both symmetric batteries are shown in Figs. 4D and E. In Fig. 4D, there is an obvious fluctuation for the battery with $MgBr_2$ electrolyte (Fig. 4D), which could be related to the incessant growth of Mg and MgO-rich SEI film [44]. Additionally, at the initial cycles, the battery with $MgBr_2$ electrolyte shows a higher overpotential than that of the battery with LiBr electrolyte, which may be associated with interfacial resistance of battery [45,46]. Due to the formation of Mg and MgO on Li anode surface, the polarization potential is greatly increased, which is similar previous work [47]. Note that the battery with LiBr electrolyte shows a drastic potential increase after 500 h (Fig. 4E). The phenomenon can be ascribed to the poor interface stability that comes from redox shuttle of Br_3^- and the accumulation of dead Li. In contrast, the overpotential of the battery using $MgBr_2$ electrolyte is reduced with the raise of cycle number, which could be caused by the formation of stable passivation layer. These results can conclude that the generation of Mg and MgO-rich SEI film is beneficial to restraining the redox shuttle of Br_3^- and improving the cycling stability of battery.

In summary, $MgBr_2$ as a self-defensed RM is firstly employed in Li-O_2 batteries. The advanced strategy effectively enhances the round-trip efficiency and extends the life time of Li-O_2 batteries due to the dual functions of $MgBr_2$. On the one hand, being a RM, the generated Br_3^- contributes to accelerating the decomposition of Li_2O_2 and thus reducing the cell overpotential. On the other hand, based on the *in-situ* spontaneous reactions of Mg^{2+} and Li anode under O_2 environment, a uniform SEI film containing Mg and MgO generates on Li anode surface, which is beneficial to restraining the redox shuttle of Br_3^- and improving the interface stability of Li anode. We hope this work could provide a new idea to inhibit the redox shuttle for RM-based Li-O_2 batteries.

Declaration of competing interest

The authors declare that they have no known competing financial interests or personal relationships that could have appeared to influence the work reported in this paper.

Acknowledgments

This work was supported by the National Natural Science Foundation of China (Nos. 21978110 and 52171210), the Jilin Province Science and Technology Department Program (Nos. YDZJ202101ZYTS047, 20220201130GX and 20200201187JC), and the Science and Technology Project of Jilin Provincial Education Department (No. JJKH20210444KJ).

Supplementary materials

Supplementary material associated with this article can be found, in the online version, at doi:10.1016/j.cclet.2023.108469.

References

[1] K. Liao, S. Wu, X. Mu, et al., Adv. Mater. 30 (2018) 1705711.
[2] Y. Zhao, W. Cheng, J. Wu, et al., Chin. Chem. Lett. 34 (2023) 107413.
[3] H. Ren, Z. Zhang, J. Zhang, et al., Rare Metals 41 (2022) 106–114.
[4] L. Ma, T. Yu, E. Tzoganakis, et al., Adv. Energy Mater. 8 (2018) 1800348.
[5] H. Jiao, G. Sun, Y. Wang, et al., Chin. Chem. Lett. 33 (2022) 4008–4012.
[6] S. Rastegar, Z. Hemmat, C. Zhang, et al., ACS Appl. Mater. Interfaces 13 (2021) 4915–4922.
[7] D. Li, Z. Kang, H. Sun, et al., Chem. Eng. J. 428 (2022) 131105.
[8] Z. Liu, Y. Lin, H. Yu, et al., Tungsten 4 (2022) 81–98.
[9] J. Zhang, B. Sun, Y. Zhao, et al., Nat. Commun. 10 (2019) 602.
[10] X. Tang, W. Zhang, L. Cao, et al., Rare Metals 41 (2021) 726–729.
[11] S. Ma, J. Wang, J. Huang, et al., J. Phys. Chem. Lett. 9 (2018) 3333–3339.
[12] J. Cao, D. Zhang, R. Chanajaree, et al., Adv. Powder Mater. 1 (2022) 100007.
[13] Y. Dou, D. Kan, Y. Su, et al., J. Phys. Chem. Lett. 13 (2022) 7081–7086.
[14] Y. Zhang, L. Wang, X. Zhang, et al., Adv. Mater. 30 (2018) 1705571.
[15] Z.F. Chen, X. Lin, H. Xia, et al., J. Mater. Chem. A 7 (2019) 14260–14270.
[16] Z. Li, J. Yang, X. Ge, et al., Nano Energy 89 (2021) 106314.
[17] Y. Dou, Z. Xie, Y. Wei, et al., Natl. Sci. Rev. 9 (2022) 795–800.
[18] E. Jónsson, J.H.J. Ellison, E. Wang, et al., J. Electrochem. Soc. 168 (2021) 030529.
[19] Y. Chen, S.A. Freunberger, Z. Peng, et al., Nat. Chem. 5 (2013) 489–494.
[20] Z.Z. Shen, S.Y. Lang, Y. Shi, et al., J. Am. Chem. Soc. 141 (2019) 6900–6905.
[21] C. Zhu, Y. Wang, L. Shuai, et al., Chin. Chem. Lett. 31 (2020) 1997–2002.
[22] J. Park, S. Lee, H.G. Jung, et al., Adv. Mater. 30 (2018) 1–13.
[23] X.P. Zhang, C.Y. Li, X.Z. Fu, et al., Funct. Mater. Lett. 14 (2021) 2130008.
[24] M. Tułodziecki, G.M. Leverick, C.V. Amanchukwu, et al., Energy Environ. Sci. 10 (2017) 1828–1842.
[25] G. Leverick, M. Tułodziecki, R. Tatara, et al., Joule 3 (2019) 1106–1126.
[26] W.J. Kwak, D. Hirshberg, D. Sharon, et al., Energy Environ. Sci. 9 (2016) 2334–2345.
[27] I. Landa-Medrano, I. Lozano, N. Ortiz-Vitoriano, et al., J. Mater. Chem. A 7 (2019) 8746–8764.
[28] C. Zheng, W. Ding, C. Wang, et al., J. Mater. Chem. A 7 (2019) 6180–6186.
[29] J. Liu, T. Wu, S. Zhang, et al., J. Power Sources 439 (2019) 227095.
[30] X. Zhang, Y. Li, J. Deng, et al., J. Power Sources 506 (2021) 230181.
[31] W. Bai, Z. Zhang, X. Chen, et al., Chem. Commun. 56 (2020) 12566–12569.
[32] Z. Huang, J. Ren, W. Zhang, et al., Adv. Mater. 30 (2018) 1803270.
[33] Z. Liang, Y.C. Lu, J. Am. Chem. Soc. 138 (2016) 7574–7583.
[34] G. Sun, R. Gao, H. Jiao, et al., Adv. Mater. 34 (2022) 2201838.
[35] T. Zhang, K. Liao, P. He, et al., Energy Environ. Sci. 9 (2016) 1024–1030.
[36] G. Ma, Z. Wen, Q. Wang, et al., J. Mater. Chem. A 2 (2014) 19355–19359.
[37] S. Aksoy, Y. Caglar, S. Ilican, et al., J. Alloys Compd. 512 (2012) 171–178.
[38] J. Muldoon, C.B. Bucur, T. Gregory, Chem. Rev. 114 (2014) 11683–11720.
[39] S. Choudhury, Z. Tu, S. Stalin, et al., Angew. Chem. Int. Ed. 56 (2017) 13070–13077.
[40] H. Cheng, B. Huang, P. Wang, et al., Chem. Commun. 47 (2011) 7054–7056.
[41] S. Xu, Z. Zhong, W. Liu, et al., Environ. Res. 186 (2020) 109489.
[42] Q. Zhao, Y. Zhang, G. Sun, et al., ACS Appl. Mater. Interfaces 10 (2018) 26312–26319.
[43] Q. Xu, J. Lin, C. Ye, et al., Adv. Energy Mater. 10 (2020) 1903292.
[44] F. Guo, T. Kang, Z. Liu, et al., Nano Lett. 19 (2019) 6377–6384.
[45] X.Q. Zhang, X.B. Cheng, X. Chen, et al., Adv. Funct. Mater. 27 (2017) 1605989.
[46] P.M. Gonzalez Puente, S. Song, S. Cao, et al., J. Adv. Ceram. 10 (2021) 933–972.
[47] W. Lu, L. Sun, Y. Zhao, et al., Energy Storage Mater. 34 (2021) 241–249.